Res Chem Intermed (2015) 41:8839–8854
DOI 10.1007/s11164-015-1932-6

Photocatalytic properties of $BiVO_4$ synthesized by microwave-assisted hydrothermal method under simulated sunlight irradiation

D. Sánchez-Martínez · D. B. Hernández-Uresti · Leticia M. Torres-Martinez · S. Mejia-Rosales

Received: 25 August 2014 / Accepted: 19 January 2015 / Published online: 25 February 2015

Abstract $BiVO_4$ with monoclinic-type structure were successfully synthesized by microwave-assisted hydrothermal method (BiMH) and hydrothermal reaction (BiH500) in aqueous medium. The materials were characterized by X-ray diffraction, scanning electron microscopy, Barrett–Emmett–Teller technique, diffuse reflectance spectroscopy, and UV–Vis spectroscopy. The photocatalytic activity of samples was evaluated by the degradation of different pollutants such as xanthene (rhodamine B), indigoids (indigo carmine), and antibiotics (tetracycline) under simulated sun-light irradiation. The relation among surface area, morphology, particle size, charge recombination, and photocatalytic performance of the powders was also discussed. The degradation of the antibiotic solution (TC) over $BiVO_4$ photocatalyst was quickly reached for with half-life time ($t_{1/2}$) minor than 12 min. On the other hand, in the case of organic dyes (RhB and IC) the best results were $t_{1/2} = 79$ and 150 min under simulated sun-light irradiation, respectively. $BiVO_4$, had a good stability, did not present photocorroded under irradiation. The degree of mineralization of the organic compounds was determined by total organic content (TOC) analysis, which revealed that mineralization by the action of BiMH is feasible in 83 % (RhB), 58 % (IC), and 50 % (TC) after 96 h of irradiation.

D. Sánchez-Martínez · L. M. Torres-Martinez
Departamento de Ecomateriales y Energía, Facultad de Ingeniería Civil, Universidad Autónoma de Nuevo León, Cd. Universitaria, C.P. 66451 San Nicolás de los Garza, NL, Mexico

D. B. Hernández-Uresti (✉) · S. Mejia-Rosales
Facultad de Ciencias Físico - Matemáticas, Universidad Autónoma de Nuevo León, Cd. Universitaria, C.P. 66451 San Nicolás de los Garza, NL, Mexico
e-mail: ing.dianahdz@gmail.com

D. B. Hernández-Uresti · S. Mejia-Rosales
Centro de Innovación, Investigación y Desarrollo en Ingeniería y Tecnología, UANL Nueva Carretera al Aeropuerto Internacional Monterrey Km 10-PIIT, Apodaca, NL 66600, Mexico

Keywords $BiVO_4$ · Microwave-assisted hydrothermal method · Heterogeneous photocatalysis · Tetracycline

Introduction

Nowadays, the use of semiconductor compounds as photocatalysts has become increasingly important in providing alternative sources of energy and problems associated with environmental fields such as wastewater treatment. These treatments have achieved an often incomplete removal of organic pollutants, resulting in discharge of these organic molecules as antibiotics and dyes into the rivers and oceans. The antibiotics are of concern due to potential genotoxic effects, disruption of aquatic ecology, and human health risks [1–3]. One of the most frequently detected antibiotics in wastewater is tetracycline [4]. Previous studies have reported the tetracycline degradation in the wastewater by different treatments such as membrane bioreactors with a tetracycline concentration of 500 $\mu g\ l^{-1}$ [5], activated sludge process (23.8–353 $ng\ l^{-1}$) [6], etc. The advanced oxidation processes (AOP's) have been reported for removal of antibiotics in wastewater effluents [7–9]. The AOP's which has gained wide attention is the heterogeneous photocatalysis due to its effectiveness in degrading and mineralizing the recalcitrant organic compounds by UV and Vis light [10]. An ideal photocatalyst should possess a high mobility for photoestimulated electron–hole separation and suitable energy levels of band potentials. This is one of the most significant considerations, as a semiconductor is chosen for the photocatalytic application. Among a variety of photocatalysts, TiO_2 appears as the most emerging destructive technology owing to outstanding chemical stability and its reliable photocatalytic activity [11–13]. However, the large band gap energy ($\sim$3.2 eV) for TiO_2 (excitation wavelength $<$380 nm) can only absorb ultraviolet light, not visible light, which limits its practical application under the condition of natural solar light [14, 15]. For this reason, researchers try to obtain photocatalysts more efficient at solar light with photocatalytic systems able to operate effectively under visible light irradiation [16–18]. $BiVO_4$ photocatalysts have gained interest due to suitable visible light-induced energy band structure. In $BiVO_4$ polymorphs exist three crystal forms including monoclinic scheelite, tetragonal scheelite, and tetragonal zircon [19–21]. Among the three crystal type structures of $BiVO_4$, monoclinic exhibits much higher photocatalytic activity than the other two tetragonal phases [22, 23]. For this reason, many authors focus their efforts on the possibility of controlling the synthesis owing to that the efficiency of the photocatalysts are associated with electronic, structural, and morphological properties of the material [24, 25].

Many methods have been employed to synthesize monoclinic $BiVO_4$ such as solid-state reaction [26], co-precipitation [27], and molten salt method [28]. However, the high energy consumption and high preparation costs have been the reason to search for an alternate wet chemical process to synthesize inorganic materials at lower temperatures such as hydrothermal [29], sonochemistry [30], solvothermal [31], and microwave irradiation method [32]. A new method of

synthesis has drawn the attention of many researchers. There are two lines of interest in microwave-assisted hydrothermal processing, one of these lines deals with processing itself, efficiency and productivity, by reducing processing temperature and time, while the second one deals with the properties of the obtained material, such as thermal diffusivity, permittivity, and other electromagnetic properties. Nowadays, few studies in the literature have focused on $BiVO_4$ synthesis by microwave-assisted hydrothermal method, as shown as Table 1. The researchers reported the photocatalytic activity of $BiVO_4$ with rhodamine B (xanthene's family) such as pollution molecule (see Table 1). In order to know the photocatalytic performance of the other pollution's families and take control of morphology and textural properties, $BiVO_4$ was synthesized by microwave-assisted hydrothermal method. The photocatalytic activity of the bismuth vanadate will be evaluated in the degradation reactions of different organic compounds families: rhodamine B (RhB, CAS 81-88-9) was used for the xanthene family, indigo carmine (IC, CAS 860-22-0) was used for indigoids family and tetracycline (TC, CAS 60-54-8) was used for antibiotic family, all of them under simulated sunlight irradiation.

Experimental

Synthesis of $BiVO_4$ powders

$BiVO_4$ powders were obtained by microwave-assisted hydrothermal method. For this purpose, 0.01 M of $Bi(NO_3)_3{\cdot}5H_2O$ (Sigma-Aldrich, 99 %) was dissolved in 50 ml of nitric acid solution (10 % v/v, HNO_3) under vigorous stirring and NH_4VO_3 (Sigma-Aldrich, 99 %) was added into the solution. Afterwards, the aqueous

Table 1 Research reported in the literature on the preparation of $BiVO_4$ via microwave-assisted hydrothermal processes

Sample	Synthesis method	Degradation	Particle size (μm)	Surface area ($m^2\ g^{-1}$)	Band gap (eV)	Reference
$TiO_2/BiVO_4$ slab-like structure	Microwave hydrothermal synthesis	RhB	0.5–7	0.70–0.92	2.04–2.17	[33]
N-doped $BiVO_4$ nanoplates	Microwave hydrothermal synthesis	RhB	0.78–0.85	1.34	2.00	[34]
$BiVO_4$ dendritic structure	Microwave-assisted hydrothermal	RhB	0.20–50	0.16–5.76	2.33–2.48	[35]
$BiVO_4$ rod-like structure	Microwave-assisted hydrothermal	RhB IC TC	0.5–0.90	3.84	2.37	This work

solution was stirred for 10 min at room temperature and the pH was adjusted to 4. The resulting solution was transferred into a microwave-assisted hydrothermal device and heated with a power of 200 W at 180 °C for 90 min. The yellow precipitate formed was washed several times with distilled water to neutralize the pH of the solution. It was then dried in air at 70 °C for 24 h. $BiVO_4$ powders were prepared by the hydrothermal method starting from aqueous solutions of $Bi(NO_3)_3$-$5H_2O$ and NH_4VO_3, as was described previously. The solution formed was transferred into a 600-ml Teflon-lined stainless-steel autoclave. The autoclave was sealed and heated at 180 °C for 90 min. Then, the autoclave was cooled to room temperature. The precipitate formed was separated by filtration, washed several times with distilled water, and dried at 70 °C for 24 h. Afterwards, the resulting powders were calcined at 500 °C for 24 h in a porcelain crucible in air for obtained the monoclinic phase.

Characterization of $BiVO_4$

Structural characterization of $BiVO_4$ was performed by X-ray powder diffraction using a Bruker D8 advanced diffractometer with Cu-K_α radiation ($\lambda = 1.5418$ Å) coupled with a Vantec high-speed detector. X-ray diffraction (XRD) data of the samples was collected in the 2θ range of 10–60° with a scan rate of 0.05° s^{-1}. The morphology of the oxides was analyzed by scanning electron microscopy (SEM) using an FEI Nova 200 NanoSEM microscope operated at low vacuum. UV–Vis diffuse reflectance absorption spectra of the samples were obtained by using a UV–Vis spectrophotometer (PerkinElmer Lambda 35) equipped with an integrating sphere and by using $BaTiO_3$ as a reference. The procedures to calculate the Eg from the UV–Vis spectrum were established in a previous work [36]. The photoluminescence (PL) emission spectra of the samples were recorded with 431 nm as an excitation light source in order to investigate the recombination of electron–hole pair in the photocatalysts. The emission from the sample was measured by a spectrometer Agilent Technologies Cary Eclipse Fluorescence Spectrophotometer. The specific surface area was determined in the equilibrium points P/P_0 ranging from 0.05 to 0.35 by the Brunauer–Emmett–Teller (BET) method in a Bel-Japan Minisorp II surface area and pore size analyzer.

Photocatalytic experiments

The rhodamine B (5 mg l^{-1}), indigo carmine (30 mg l^{-1}) and tetracycline (20 mg l^{-1}) reactions were performed using a borosilicate reactor (300 ml) equipped with a circulating cooling water system. The simulated sunlight irradiation source used was a xenon lamp (6,000 K). In the oxidation experiment, 200 mg of the photocatalyst was dispersed in 200 ml of the solution. This solution was sonicated 1 min and kept in dark conditions for 1 h to ensure the equilibrium adsorption–desorption of organic compound on the catalyst surface were reached. After this time, the light source was turned on. The samples were taken from the reactor at different time intervals and then analyzed following the procedures established in a previous work [37]. The mineralization degree was monitored by

analyzing the total organic carbon content (TOC) in the solutions at different irradiation times. In the mineralization experiment, 250 ml of the corresponding solution (50 mg l^{-1} for RhB and TC; and 30 mg l^{-1} for IC) containing 250 mg of photocatalyst was employed. The aliquots were analyzed in a Shimadzu VSCN8 total organic content (TOC) analyzer.

Results and discussion

Characterization

The m-$BiVO_4$ phase synthesized by hydrothermal and microwave-assisted hydrothermal method was investigated by XRD. In the microwave hydrothermal method, all diffraction peaks can be indexed on the pure the monoclinic scheelite structure of $BiVO_4$ without impurities or other phases, as shown in Fig. 1. The profile of the diffraction peaks indicates that the powders are well crystallized and are in agreement with the reported data in the respective JCPDS card No. 01-075-1867. These samples don't need thermal treatment to obtain the monoclinic phase, which implies changes in the surface area due to the when increase the temperature calcination leads to decrease the surface area of the sample. The $BiVO_4$ prepared by hydrothermal reaction showed diffraction peaks of a crystal mixture consisting of tetragonal (*t*-) and monoclinic (*m*-) structures, as shown in Fig. 1. Because of this, the hydrothermal sample was calcined at high temperatures with the purpose of eliminating the tetragonal phase in the powder. The percentage of monoclinic phase has been calculated based on the normalized ratios of relative intensities for (2 0 0)

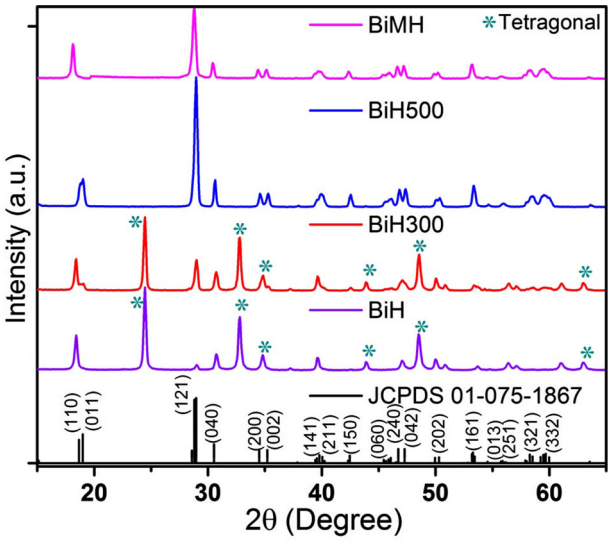

Fig. 1 X-ray diffraction patterns of $BiVO_4$ samples obtained by microwave-assisted hydrothermal method and hydrothermal reaction at different temperature of calcination

at $2\theta = 24.47°$ peak of tetragonal $BiVO_4$ and (1 2 1) at $2\theta = 28.95°$ peak of monoclinic $BiVO_4$ [38]:

$$V_{\text{mono}} = \frac{I_{\text{mono}(121)}}{I_{\text{mono}(221)} + I_{\text{tetra}(200)}}$$

where V_{mono} is the weight fraction of monoclinic phase in the powder, $I_{\text{mono}(1\ 2\ 1)}$ and $I_{\text{tetra}(2\ 0\ 0)}$ are the X-ray intensities of the monoclinic and the tetragonal peaks, respectively. The content of the monoclinic phase in the powder BiH was estimated to be 5.79 % and BiH300 was estimated to be 30.26 %. The monoclinic phase of the sample prepared via hydrothermal was observed without the presence of other phases, after thermal treatment at 500 °C. The intensity diffraction patterns of the BiH500 sample revealed the higher crystallization degree. The crystallite size can be determined from the broadening of corresponding X-ray spectral peaks by Scherrer formula:

$$L = \frac{K\lambda}{(\beta \cos\theta)}$$

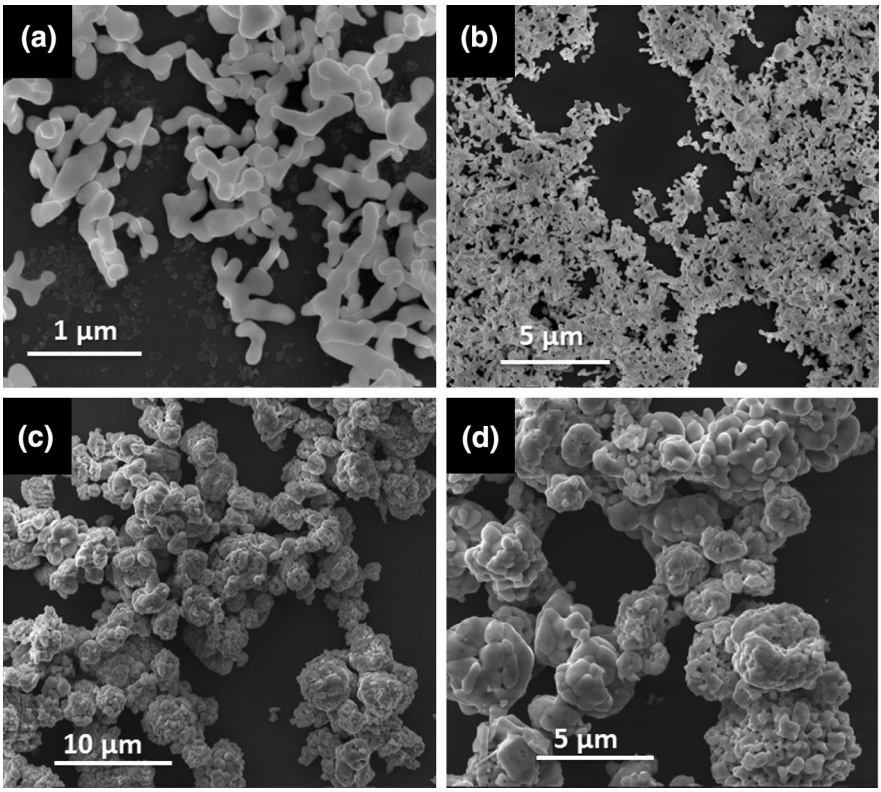

Fig. 2 SEM images of the morphology of $BiVO_4$ synthesized by **a**, **b** microwave-assisted-hydrothermal method, and **c**, **d** hydrothermal reaction

where L is the crystal size, λ is the wavelength of the X-ray radiation (Cu-$K\alpha = 1.5418$ Å), K is a constant usually taken as 1, and β is the line width at half-maximum height, after subtraction of equipment broadening. The average crystal size of monoclinic $BiVO_4$ prepared by hydrothermal method (BiH500) was estimated to be about 33 nm, which was bigger than monoclinic $BiVO_4$ (30 nm) prepared by the microwave-assisted hydrothermal method (BiMH). The band gap (Eg) of the semiconductor usually plays an important role in its photocatalytic activity, Eg for $BiVO_4$ were analyzed by UV–Vis diffuse reflectance spectroscopy (DRS). As is well known, the valence band (VB) of $BiVO_4$ is formed by Bi 6*s* and O 2*p* hybrid orbitals and the conduction band (CB) is formed by V 3*d* orbitals, so the migration of electron to formed electron–hole pair could be occur from Bi 6*s* and O 2*p* hybrid orbitals to V 3*d* orbital [39]. The band gap values obtained from the intersection of the tangents to the plots were 2.37 and 2.39 eV for $BiVO_4$ powders prepared by

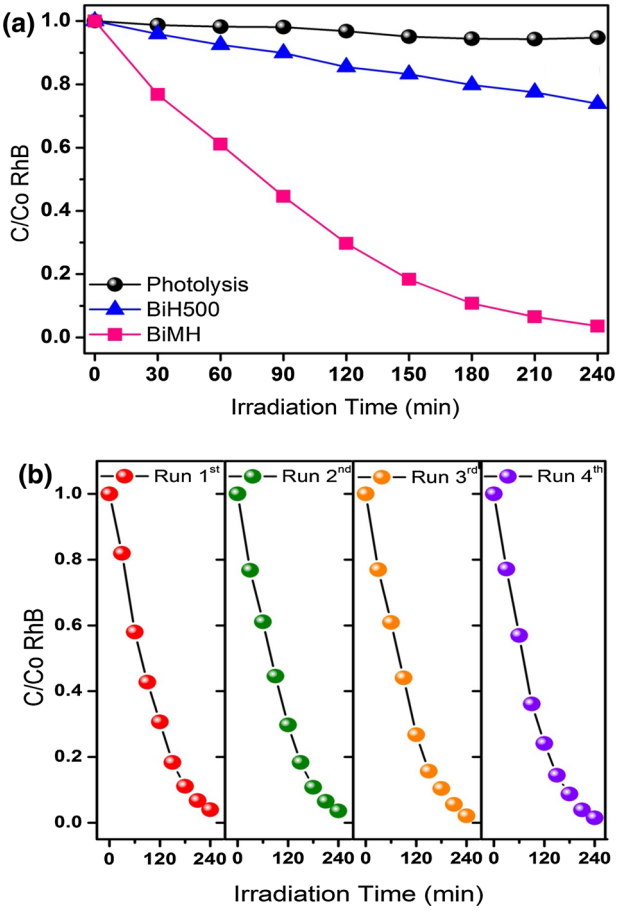

Fig. 3 Photocatalytic degradation (**a**) of RhB solution (5 mg l^{-1}) and the photostability experiments (**b**) in presence of BiMH as a photocatalyst under simulated sunlight irradiation

hydrothermal reaction (BiH500) and microwave-assisted hydrothermal method (BiMH), respectively. The Eg value of BiMH increased than Eg value of BiH500, which could be attributed of its nanosized structure could be caused a possible quantum confinement effects [35]. The BET analysis indicated a surface area value of 3.84 $m^2\ g^{-1}$ obtained for the sample prepared at 180 °C by the microwave-assisted hydrothermal method was higher than that of the sample synthesized at 180 °C by hydrothermal reaction of 1.30 $m^2\ g^{-1}$, which it was heat treatment at 500 °C to obtained the monoclinic structure. The morphology and particle size of the m-$BiVO_4$ was characterized by SEM and some micrographs are shown in Fig. 2. An irregular shape was observed in the particles of the microwave-assisted

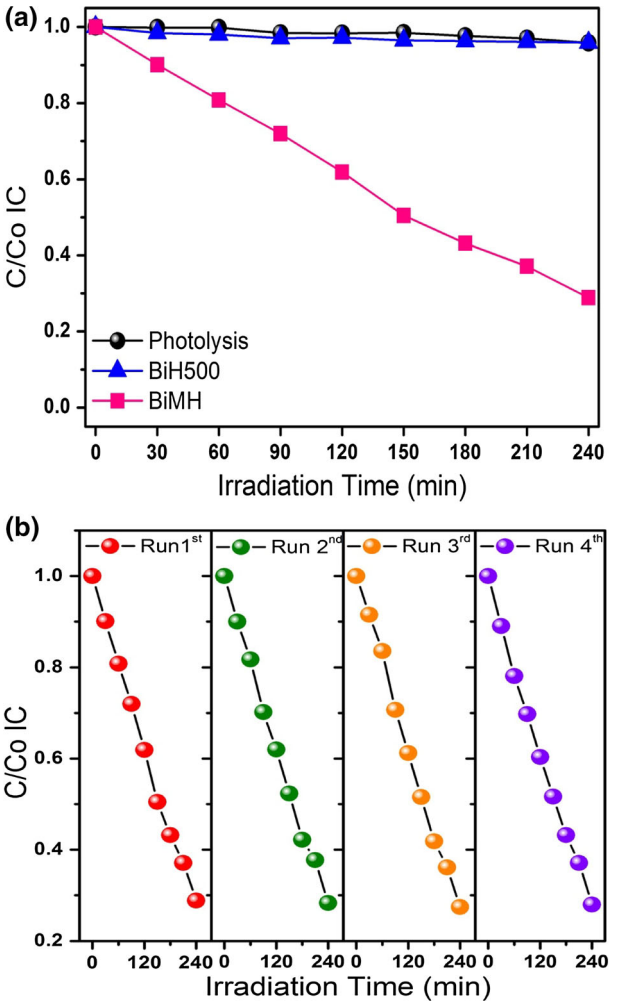

Fig. 4 Photocatalytic degradation (**a**) of IC solution (30 mg l^{-1}) and the photostability experiments (**b**) in the presence of BiMH as a photocatalyst under simulated sunlight irradiation

hydrothermal method, an incipient tendency of them to form an heterogeneous rod-like structured material, which average sizes around 600 nm, as is shown in Fig. 2a, b. Nevertheless, SEM images taken for m-$BiVO_4$ hydrothermal reaction sample are presented the roundish aggregates structured, which sizes around 5 μm, formed by irregular particles around of 1 μm, can be observed in the Fig. 2c, d. These aggregates were generated due to the calcination of the hydrothermal sample to obtain the monoclinic phase. It can be noticed that the characterization of samples by SEM is consistent with results obtained by BET analysis. It is possible to appreciate a slight decrease in surface area value, inversely to crystallinity and particle size, as

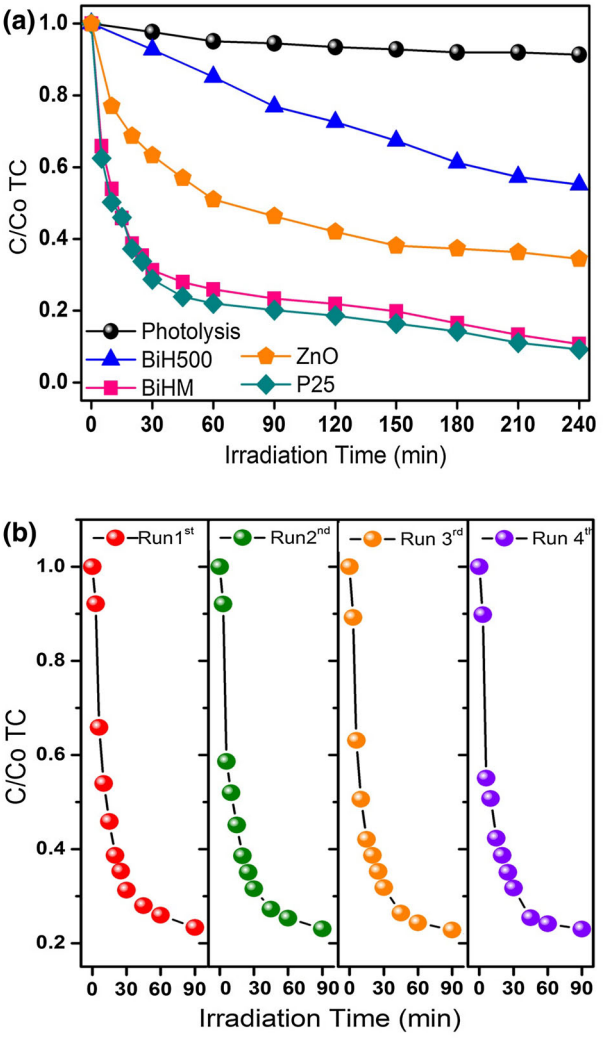

Fig. 5 Photocatalytic degradation (**a**) of TC solution (20 mg l^{-1}) and the photostability experiments (**b**) in presence of BiMH as a photocatalyst under simulated sunlight irradiation

the calcination temperature increases. $BiVO_4$ prepared by microwave-assisted hydrothermal method exhibited the largest surface area and the smallest grain size, which could be expected since the reaction took place in a solution without calcination. Clearly, the different routes induce different morphologies and sizes of the particles.

Photocatalytic experiments

In order to evaluate the photolysis degree of the organic solution under simulated sunlight irradiation, an experiment without photocatalyst was carried out, as shown in Figs. 3, 4, and 5. The concentration remained constant at all times for the rhodamine B (RhB), indigo carmine (IC), and tetracycline (TC), which indicates that the photocatalyst-irradiation combination is necessary to eliminate the organic compound from the solution in each case. In the first instance, Fig. 3a shows the photocatalytic performance of the $BiVO_4$ for the degradation of rhodamine B, an organic dye of the family of xanthene. After 240 min of exposure to lamp irradiation, the photocatalyst obtained by hydrothermal sample degraded only 27 % with the half-life time ($t_{1/2}$) = 500 min. Nevertheless, when used the microwave-assisted hydrothermal (BiMH) such as photocatalyst, the RhB solution was bleached to a large degree and half-life time for bleaching the color was 79 min. It can be seen that the degradation rate BiMH sample enhanced six times than BiH500 sample as photocatalyst, owing to the decrease particle size and the morphology plays an important role in the photocatalysis process. BiH500 crystallite size is relatively larger than BiMH, the electron–hole pairs could recombine within the particle volume before reaching the surface due to the increase in the migration distance [40–42]. When the grain size decreases, it will reduce the recombination opportunities of the electron–hole pairs in the volume, which can effectively migrate to the surface and interact with the organic compound. On other hand, RhB present two photocatalytic mechanisms at the same time for increasing the degradation rate of the organic molecule. One mechanism is the photocatalytic which $BiVO_4$ generated the electron–hole pairs by light irradiation. Electrons of the conduction band react with the O_2 molecules to yield the O_2^- radical anion. Then, several reactions generated $^{\cdot}OH$ radicals, which decomposed the organic molecule to carbon dioxide and water. The other mechanism is the photosensitization; RhB absorb visible light irradiation, which leads to an electron transfer process from excited dye to the $BiVO_4$ conduction band to initiate redox reactions for the formation of the $^{\cdot}OH$ radicals [43]. Besides, IC dye was chosen inside the indigoid family for the purpose of evaluating its photocatalytic performance, as seen at Fig. 4a. BiMH exhibited the highest photocatalytic activity, degraded 72 % after 240 min of simulated sunlight irradiation with $t_{1/2}$ = 150 min, than BiH500. The photocatalytic activity of BiMH sample increased 14 times that of BiH500. In the case of BiH500, which were synthesized by the hydrothermal method, the photoactivity were similar to photolysis of IC. Therefore, the photocatalytic activity of the BiH500 sample is void in the indigoid family. This observation indicates that the photosensitization mechanism plays an important role in the degradation of the RhB dye molecules but did not present in the IC dye. Also, the differences of

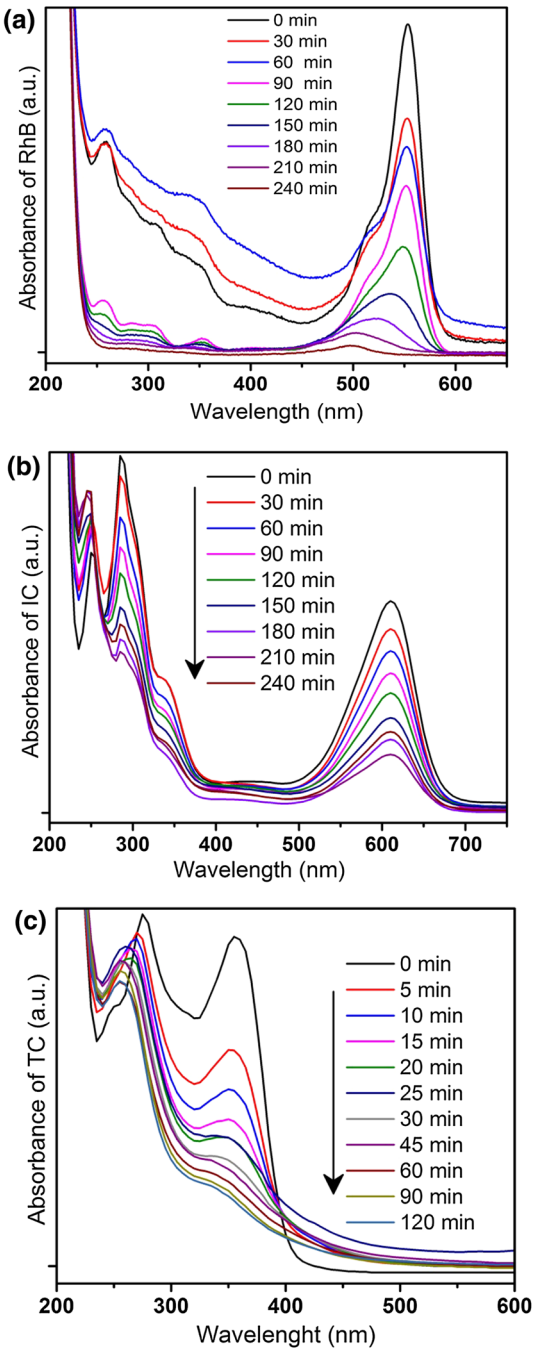

Fig. 6 Variation of the UV–Vis absorption spectra of rhodamine B (**a**), indigo carmine (**b**), and tetracycline (**c**) solution at 5, 30, and 20 mg l^{-1}, respectively

textural and morphological properties such as crystallinity degree, particle size, and surface area had an influence on the photodegradation of the organic molecule. The purpose of knows the photocatalytic activity of $BiVO_4$ in the antibiotics, tetracycline (TC) is used as organic pollutant, as shown in the Fig. 5a. The employed catalysts is BiH500 degrade 55 % after 240 min with the $t_{1/2} = 270$ min, indicated that is better for the antibiotics degradation than dyes degradation. BiMH shows a quick reduction in the first 30 min of irradiation with the $t_{1/2} = 12$ min and after tend to be stable behavior. The obvious increment in the photocatalytic activity with the both catalysis BiH500 and BiMH indicate that the broken of the molecular structure of tetracycline is feasible in the presence of $BiVO_4$ photocatalyst, but the formations of stable intermediates tend to stop the degradation reaction. This behavior could be attributed to the chemical structure of the organic compounds and the efficiency combination of their physical properties such as surface area, low charge recombination, particle sizes, and morphology [44]. The efficient combination of these parameters should operate in BiMH to improve the photocatalytic activity due to be related to the efficiency of the electron–hole separation. In this sense, if the particle size decreases, it will reduce the pathway from the site of generation of the electron–hole pairs to the photocatalyst surface, so the recombination opportunities will be reduced as well. The ZnO and TiO_2 photocatalytic tests have been added in Fig. 5a in order to compare the efficiency of the catalyst that presented the best photoactivity (BiMH) with the oxides more cited by the researchers. The BiMH presented a higher photoactivity than ZnO but similar photoactivity to TiO_2 for TC solution after 240 min under sunlight simulation. The ZnO and TiO_2 oxides exhibited photocatalytic performance because the Xe lamp is heterochromatic spectra with low UV irradiation, enough to activate oxides. In conclusion, the $BiVO_4$ photocatalyst is a good candidate to pharmaceutical compounds degradation in water. Figure 6 describes the UV–Vis absorbance spectra of RhB, IC, and TC solution over BiMH sample, used as photocatalyst, exhibiting the best photocatalytic activity. It is notable that the UV–Vis absorption

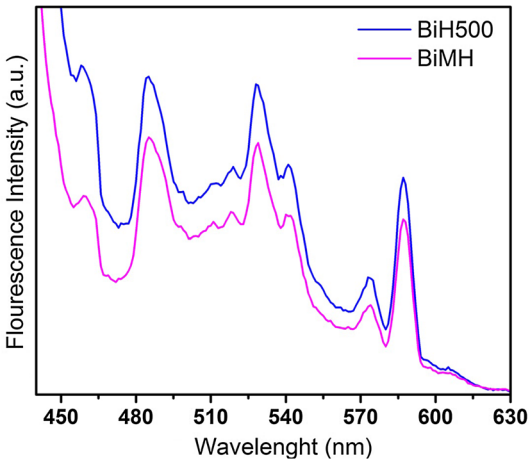

Fig. 7 Photoluminescence spectra of $BiVO_4$ samples

spectra of three pollutants were decreased over time, may be caused for a direct attack to the aromatic rings of its molecule, which are completely decomposing into small organic/inorganic molecules or/and ions products [45]. Photoluminescence (PL) spectroscopy could be used to determinate the efficiency of charge carrier migration, trapping, and transfer, for determinate the recombination of the electron–hole pairs in semiconductor [46]. Figure 7 shows the comparison of PL spectra of monoclinic BiMH and monoclinic BiH500 at 431 nm as wavelength excitation. PL intensity of the BiMH sample is lower than that of BiH500, which implies that the recombination electron in the V 3*d* of CB and hole in the O 2*p* in VB was diminished under light irradiation, which corresponds to the 483-nm peak [47]. It indicates the best promoting efficiency of generate the electron–hole pair to the surface of the semiconductor and attack to the organic compounds. In other hand, BiMH was probably more active sites on the surface for the oxidation of the pollutant molecules [48] than the BiH500 sample. The material obtained by hydrothermal method had a big roundish aggregate structure, almost aggregates with the smooth surface. Forasmuch as, the microwave irradiation increasing rapidly the synthesis temperature during the nucleation phase and with the air flow causes the fast decreasing of temperature in the solution. These actions minimize size distributions owing to the quenching. The BET area analysis revealed that the BiMH sample exhibited specific surface area three times higher than the one observed for the BiH500 sample. For a photocatalyst to be useful, it should be stable under repeated applications. To test the repeatability of organic compound degradation using the BiMH as the same photocatalyst powder, we carried out the experiment repeatedly four times. Figure 3b shows the high stability of BiMH as photocatalyst in the degradation of the RhB, maintaining the efficiency of $t_{1/2}$ around 80 min. The recycled experiments for the photodegradation of IC and TC experiments were performed using BiMH as a photocatalyst under simulated sunlight irradiation and did not exhibit any loss in the photocatalytic activity, as shown in Figs. 4b and 5b. The XRD pattern of the BiMH sample before and after

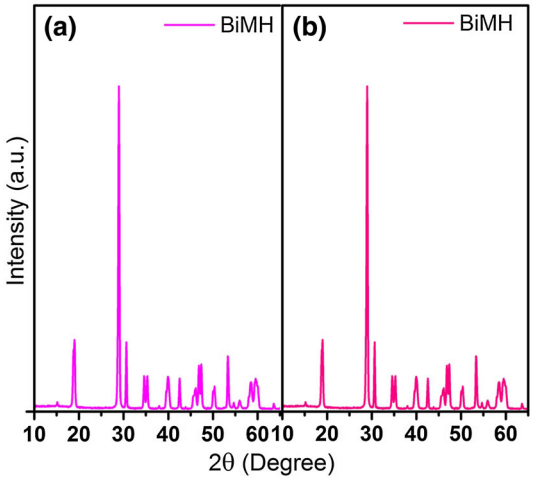

Fig. 8 X-ray diffraction patterns of $BiVO_4$ samples obtained by microwave-assisted hydrothermal method using as photocatalyst, before (**a**) and after (**b**) the recycling experiments

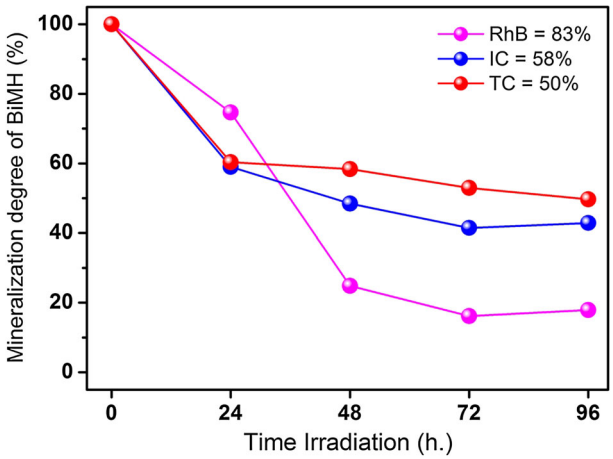

Fig. 9 Variation of the TOC during the mineralization of RhB, IC, and TC under simulated sun-light irradiation

the repeated experiment is almost identical to that of the as-prepared sample (Fig. 8). Therefore, $BiVO_4$ is an active photocatalyst and showed a high stability without photocorrosion during the photocatalytic oxidation of the organic molecules under simulated sunlight irradiation. To determine that the mineralization degree of the organic compounds by m-$BiVO_4$ is feasible, TOC analyses were performed for the degradation of RhB, IC, and TC at different simulated sunlight irradiation times, as is shown in Fig. 9. The bleaching of the dye solution is beyond the inactivation of the chromophore groups in the molecular structure of dyes. Besides, the bleaching of a solution does not imply the mineralization of the dye. The initial concentration of RhB, IC, and TC were 50, 30, and 50 mg l^{-1}, respectively. $BiVO_4$ obtained by microwave-assisted hydrothermal method as used as a photocatalyst in TOC experiments showed the highest photocatalytic activity. The mineralization degrees were 83 % for RhB, 58 % for IC, and 50 % for TC after 96 h of simulated sunlight irradiation. After 24 h, the important decrement in the TOC content was reached of TC and IC. After this time, the TOC content tends to have a semi-constant value in the TC and IC solutions. In the RhB case, the TOC content shows an important reduction in the first 48 h of irradiation. This behavior can be indicated several reaction intermediates formed, when the complex molecule is broken. The recalcitrant behavior of the chemical intermediates formed, such as organic acids of lower molecular weight, diminishes the photocatalytic degradation rate at longer reaction times. The mineralization degree corroborates the application of $BiVO_4$ in the removal of the organic compounds studied.

Conclusions

In summary, the monoclinic scheelite structured $BiVO_4$ was successfully prepared by microwave-assisted hydrothermal method and provided an efficient and fast

process according to the key principles of green chemistry. BiMH rod-like structure exhibited good capacity to degrade different organic compound families such as xanthene, indigoid, and antibiotic under simulated sunlight irradiation compared to the sample obtained by simple hydrothermal method sample, owing to the physical properties such as small particle size, high surface area, an appropriate band gap, and low recombination charges. Furthermore, BiMH can be recycled as a photocatalyst for photodegradation cycles, demonstrating high stability after four cycles of RhB, IC, and TC reaction. In addition, the mineralization of different kinds of organic molecules families over $BiVO_4$ photocatalyst is feasible. The photocatalytic activity of BiMH was higher than ZnO and similar to TiO_2 under simulated sunlight irradiation. Therefore, it can be a good candidate as a photocatalyst. This work provides the photoactivity of $BiVO_4$ in the degradation not only of rhodamine B but also the indigo carmine and tetracycline, opening up the possibility of using this photocatalyst in the mineralization of other pollution compounds.

Acknowledgments We wish to thank the Universidad Autónoma de Nuevo León (UANL) for its invaluable support through the Project PAICYT 2012 and to CONACYT for support the Project "CB2013 No. 220792", Grant "Retención No. 206863", "CB2013 No. 220802" and SEP for support of Project PROMEP/103.5/13/6644 UANL-PTC-744.

References

1. N.M. Roden, E.V. Sargent, G.T. DiFerdinando Jr, Hum. Ecol. Risk Assess. Int. J. **21**(1), 280–295 (2015)
2. A.K. Venkatesan, R.U. Halden, Sci. Rep. **4**, 3731 (2014)
3. C.G. Daughton, T.A. Ternes, Environ. Health Perspect. **107**, 907–938 (1999)
4. A.J. Watkinson, E.J. Murbyc, S.D. Costanzoa, Water Res. **41**, 4164–4176 (2007)
5. S. Xia, R. Jia, F. Feng, K. Xie, H. Li, D. Jing, X. Xu, Bioresour. Technol. **106**, 36–43 (2012)
6. B. Li, T. Zhang, Chemosphere **83**, 1284–1289 (2011)
7. S. Sarkar, S. Ali, L. Rehmann et al., J. Hazard. Mater. **278**, 16–24 (2014)
8. I. Michael, E. Hapeshi, C. Michael, A.R. Varela et al., Water Res. **46**, 5621–5634 (2012)
9. E.S. Elmolla, M. Chaudhuri, Desalination **272**, 218–224 (2011)
10. J. Choi, H. Lee, Y. Choi, S. Kim et al., Appl. Catal. B Environ. **147**, 8–16 (2014)
11. S.G. Kumar, L.G. Devi, J. Phys. Chem. A **115**, 13211–13241 (2011)
12. Z. Liu, X. Dong, Z. Liu, Q. Liu, Adv. Mater. Res. **807**, 402–409 (2013)
13. M. Takeuchi, M. Matsuoka, M. Anpo, Res. Chem. Intermed. **38**(6), 1261–1277 (2011)
14. H. Trabelsi, M. Khadhraouia, O. Hentatia, M. Ksibia, Toxicol. Environ. Chem. **95**, 543–555 (2013)
15. J.B. Joo, Q. Zhang, M. Dahl, I. Lee, J. Goebl, F. Zaera, Y. Yin, Energy Environ. Sci. **5**, 6321–6327 (2012)
16. C. Gómez-Solís, D. Sánchez-Martínez, I. Juárez-Ramírez, A. Martínez-de la Cruz, L.M. Torres-Martínez, J. Photochem. Photobiol. A Chem. **262**, 28–33 (2013)
17. F. Zhang, K. Maeda, T. Takata, T. Hisatomi, K. Domen, Catal. Today **185**, 253–258 (2012)
18. Y. Zhang, Y. Zhu, J. Yu, D. Yang, T.W. Ng, P.K. Wong, C.Y. Jimmy, Nanoscale **5**, 6307–6310 (2013)
19. Y. Cheng, J. Chen, X. Yan, Z. Zheng, Q. Xue, RSC Adv. **3**, 20606–20612 (2013)
20. R.L. Frost, D.A. Henry, M.L. Weier, W. Martens, J. Raman Spectrosc. **37**, 722–732 (2006)
21. M. Dragomir, I. Arčona, S. Gardonio, M. Valant, Acta Mater. **61**, 1126–1135 (2013)
22. W. Yin, W. Wang, L. Zhou, S. Sun, L. Zhang, J. Hazard. Mater. **173**, 194–199 (2010)
23. B Cheng, W Wang, L Shi, J Zhang, J Ran, H Yu (2012) Int J Photoenergy. Article ID 797968
24. S. Mozia, A. Heciak, A.W. Morawski, Appl. Catal. B Environ. **104**, 21–29 (2011)
25. J. Hou, Y. Qu, D. Krsmanovic, C. Ducati, D. Eder, R.V. Kumar, J. Mater. Chem. **20**, 2418–2423 (2012)

26. M. Shang, W. Wang, J. Ren, S. Sun, L. Zhang, CrystEngComm. **12**, 1754–1758 (2010)
27. J. Yu, Y. Zhang, A. Kudo, J. Solid State Chem. **182**, 223–228 (2009)
28. Y. Liu, J. Ma, Z. Liu, C. Dai, Z. Song, Y. Sun, J. Fang, J. Zhao, Ceram. Int. **36**, 2073–2077 (2010)
29. S. Obregón, A. Caballero, G. Colón, Appl. Catal. B Environ. **117–118**, 59–66 (2012)
30. Y. Shi, C. Zhu, L. Wang, C. Zhao, W. Li, K.K. Fung, T. Ma, A. Hagfeldt, N. Wang, Chem. Mater. **25**, 1000–1012 (2013)
31. L. Ma, W.-H. Lia, J.-H. Luo, Mater. Lett. **102–103**, 65–67 (2013)
32. W. Shi, Y. Yan, X. Yan, Chem. Eng. J. **215–216**, 740–746 (2013)
33. L. Zhang, G. Tan, S. Wei, H. Ren, A. Xia, Y. Luo, Ceram. Int. **39**, 8597–8604 (2013)
34. G. Tan, L. Zhang, H. Ren, J. Huang, W. Yang, A. Xia, Ceram. Int. **40**, 8597–8604 (2014)
35. G. Tan, L. Zhang, H. Ren, S. Wei, J. Huang, A. Xia, ACS Appl. Mater. Interfaces **5**, 5186–5193 (2013)
36. D.B. Hernández-Uresti, A. Martínez-de la Cruz, J.A. Aguilar-Garib, Catal. Today **212**, 70–74 (2013)
37. M. Oshikiri, M. Boero, J. Ye, Z. Zou, G. Kido, J. Chem. Phys. **117**, 7313–7318 (2002)
38. L. Zhou, W. Wang, S. Liu, L. Zhang, H. Xu, W. Zhu, J. Mol. Catal. A: Chem. **252**, 120–124 (2006)
39. W. Liu, Y. Yu, L. Cao, G. Su, X. Liu, L. Zhang, Y. Wang, J. Hazard. Mater. **181**, 1102–1108 (2010)
40. T. Preethi, B. Abarna, K.N. Vidhya, G.R. Rajarajeswarin, Ceram. Int. **40**, 13159–13167 (2014)
41. X. Zhu, Q. Hang, Z. Xing et al., J. Am. Ceram. Soc. **94**, 2688–2693 (2011)
42. C. Hao, Fusheng Wen, J. Xiang et al., Mater. Res. Bull. **50**, 369–373 (2014)
43. H.H. Mohamed, D.W. Bahnemann, Appl. Catal. B Environ. **128**, 91–104 (2012)
44. C. Karunakaran, S. Kalaivani, P. Vinayagamoorthy, S. Dash, Mater. Sci. Semicond. Process. **21**, 122–131 (2014)
45. C. Li, G. Chen, J. Sun, Y. Feng et al., Appl. Catal. B Environ. **163**, 415–423 (2015)
46. C. Li, G. Chen, J. Sun, H. Dong et al., Appl. Catal. B Environ. **160–161**, 383–389 (2014)
47. C. Yu, K. Yang, J.C. Yu, F. Cao, X. Li, X. Zho, J. Alloys Compounds **50**, 4547–4552 (2011)
48. Y. Qu, W. Zhou, Z. Ren, S. Du, X. Meng et al., J. Mater. Chem. **22**, 16471–16476 (2012)